Numerical methods for fluctuation-driven interactions between dielectrics

S. Pasquali,[1] F. Nitti,[2] and A. C. Maggs[1]
[1]*Laboratoire de Physico-Chime Théorique, UMR Gulliver CNRS-ESPCI 7083, 10 rue Vauquelin, 75231 Paris Cedex 05, France*
[2]*CPHT, Ecole Polytechnique, 91128, UMR du CNRS 7644, Palaiseau, France*
(Received 9 March 2007; published 14 January 2008)

We develop a discretized theory of thermal Casimir interactions to numerically calculate the interactions between fluctuating dielectrics. From a constrained partition function we derive a surface free energy, while handling divergences that depend on system size and discretization. We derive analytic results for parallel plate geometry in order to check the convergence of the numerical methods. We use the method to calculate vertical and lateral Casimir forces for a set of grooves.

DOI: 10.1103/PhysRevE.77.016705 PACS number(s): 05.10.−a, 41.20.Cv

I. INTRODUCTION

Dispersion forces are long-range interactions due to thermal or quantum fluctuation fields. The first theoretical derivation was due to Casimir [1], who predicted the attraction of two neutral plates. A general continuum theory, developed by Lifschitz [2], addresses the nonadditivity of these forces and is often used to interpret experiments [3]. Calculation of dispersion forces requires knowledge of the frequency dependent dielectric constant, information which is accessible from spectroscopy. The results of the theory can be expressed as a sum over Matsubara frequencies [4]. However, one can isolate the zero Matsubara frequency and recognize that the corresponding contribution is both temperature dependent and independent of $\hbar$; it is purely classical and depends on the static dielectric constant, $\epsilon(\omega=0)$. The forces derived from all other frequencies depend on dynamic dipole fluctuations and require information on the frequency dependence of the dielectric permittivity. For biophysical systems, mainly composed of water and lipids, Ninham and Parsegian [5,6] have shown that zero frequency gives a contribution to the interaction which is at least as important as the interactions coming from the UV region of $\epsilon(\omega)$. This feature makes biological materials rather unique, and justifies the study of the zero frequency contribution alone. Zero Matsubara frequency forces go under different names including static van der Waals forces [7], classical thermal Casimir forces [8], and Keesom interactions. For the simplest geometries one can calculate the free energy analytically [9,10].

For more complex geometries this problem has been approached from various directions, both in its full quantum formulation, and in the high temperature, classical, regime. The range of techniques used is very wide, including Green's function formulations [11], worldline numerics [12], and path-integral formulations [13]. These techniques have allowed for great progress in linking the theory with experimental observation, but, as of now, no general method is available for arbitrary geometries and arbitrary values of the parameters.

Recently, there has been a renewed interest in Casimir forces among soft condensed matter physicists as it was recognized that these forces can play an important role in biophysical systems [7,8]. Ninham and Parsegian observations have opened the road for new formulations of dispersion forces that focus exclusively on their classical part. Dean and Horgan showed how to calculate the free energy using a classical partition function without the machinery of Matsubara frequencies [8]. This formulation has the advantage of making the physics more transparent, as thermal effects are considered explicitly from the start, rather than obtained as a limiting case of a quantum theory.

In order to address a wider variety of geometries than is possible analytically, we introduce numerical methods that can be used to study thermal Casimir forces on a lattice. The latter should be thought of as a mathematical discrete grid with no physical meaning. It is introduced to implement the numerical algorithms, and its spacing should be much smaller than the typical size of the system under investigation. In particular we address the nature of the various terms appearing in the free energy of a dielectric system and study their variation with the discretization. This corresponds to the issue of regularization of divergences in a continuous infinite system. We apply our methods to a set of rectangular and sinusoidal grooves in order to characterize both longitudinal and transverse Casimir interactions.

In this paper we are interested in computing the free energy due to thermal fluctuations of the electrostatic field between dielectric bodies. In this classical perspective, as noted above, the dielectric permittivity ϵ is taken to be a function of space, $\epsilon(r)$, but not a function of frequencies, i.e., $\epsilon(r,\omega=0)$. Our main goal is to develop a formalism which is a suitable starting point for efficient and versatile numerical methods, which can be applied to arbitrary geometries. Considering the classical, time-independent regime alone, allows us to present the general formulation and the numerical approaches on the simplest system. After a calibration which is run with convenient but nonphysical values of $\epsilon(r)$, we focus on systems with physically relevant material properties, that is systems for which the optical properties of the object immersed in water match those of water. This is the case if we choose a material whose refractive index is similar to that of water, $n\sim 1.3$, giving a dielectric constant for the material of $\epsilon_{mat}=1.7$, while $\epsilon_{H_2O}\sim 80$.

In separate works we extend our approach to quantum regimes, considering the full dielectric function $\epsilon(r,\omega)$ [14]. There, we also compare our method with other discretized numerical approaches that have recently appeared [15]. We note also the existence of a second regime where thermal

interactions can dominate even in the absence of matching of optical properties [16]; separations L satisfy $L \gg \hbar c/(2k_BT)$. This case is only relevant when $L \gg 4$ μm and will not be discussed further here.

The paper is organized as follows: In Sec. II we discretize a set of dielectrics and derive the main theoretical results; in Sec. III we study the discretized system using matrix diagonalization and Monte Carlo simulation. In Sec. IV we present a continuum calculation which derives the free energy of a single homogeneous slab with periodic boundary conditions. This result is compared to the numerical results in Sec. V, where we also show how the numerical methods can be used to calculate the free energy for grooved surfaces.

II. LATTICE FORMULATION

The free energy of a dielectric in the absence of free charges is calculated from the partition function [17]

$$\mathcal{Z} = \int \mathcal{D}[\mathbf{D}] \prod_r \delta(\nabla \cdot \mathbf{D}) e^{-\beta \mathcal{U}}, \tag{1}$$

with $\mathbf{D}(\mathbf{r})$ the electric displacement. The Boltzmann factor is the electrostatic energy in the presence of a dielectric medium $\mathcal{U} = \int [\mathbf{D}^2(\mathbf{r})/2\epsilon(\mathbf{r})] d^3\mathbf{r}$. Gauss' law $\nabla \cdot \mathbf{D} = 0$ is imposed in Eq. (1) as a constraint. In the continuum limit, and also in infinite volume, Eq. (1) is ill defined, as it contains divergences. We thus discretize in order to find an unambiguous definition of the free energy. We will then remove contributions to the free energy that diverge when the system size diverges, or mesh size is taken to zero, in order to calculate the remaining long-ranged contributions to the free energy.

We use a cubic lattice of N nodes and $3N$ links. Since we are discretizing a macroscopic theory our lattice is not related to a physical atomic lattice. To be meaningful the lattice spacing should be large compared to atomic dimensions (so that one can discuss electrostatic interactions in terms of a dielectric constant), but small compared to the physical system at hand. The specific value of the lattice spacing can be varied until convergence is achieved. We illustrate this point in Fig. 4 and related discussion where we compare numerical and theoretical results. For simplicity of notation we set the lattice spacing equal to 1 and work in arbitrary units all through the paper. Physical results depend on the ratio between the size of the bodies and their separation. Dimensional information can be reintroduced by standard scaling arguments. Physical quantities are associated with nodes or links; scalars "live" on nodes, vectors on links. Thus D_{nx} is assigned to the link leaving the node n in the positive x direction. The discretized divergence $\nabla \cdot \mathbf{D}$ gives the total flux at a lattice site. The dielectric permittivity ϵ is also associated with the links so that the discretized energy density takes the form $\frac{D_x^2}{2\epsilon_x} + \frac{D_y^2}{2\epsilon_y} + \frac{D_z^2}{2\epsilon_z}$. On a lattice, Eq. (1) becomes

$$\mathcal{Z} = \int \mathcal{D}[\mathbf{D}] \left(\prod_{nodes}^{N-1} \delta(\nabla \cdot \mathbf{D}) \right) \exp\left(-\frac{\beta}{2} \sum_{links} \frac{D_l^2}{\epsilon_l} \right), \tag{2}$$

where ϵ_l is the permittivity associated with the link l. Notice that in periodic boundary conditions we impose $N-1$ δ functions; the constraint on the Nth node is automatically satisfied when $N-1$ are imposed since $\int \nabla \cdot \mathbf{D} d^3\mathbf{r} = 0$.

We impose Gauss' law by introducing an auxiliary scalar field $\phi \equiv \{\phi_n\}_{n=1\ldots N}$ as a Lagrange multiplier, using the identity

$$(2\pi)^N \prod_{nodes} \delta(\nabla \cdot \mathbf{D}) = \int \mathcal{D}[\phi] \exp\left(-i \sum_{nodes} \phi \nabla \cdot \mathbf{D} \right). \tag{3}$$

It was shown in [18] that ϕ is the static electrostatic potential. This identity involves the product over all N nodes, so we must introduce an extra constraint $\delta(\phi_N)$ to remove the integral over ϕ_N. Dropping irrelevant prefactors, Eq. (2) becomes

$$\mathcal{Z} = \int \mathcal{D}[\phi] \mathcal{D}[\mathbf{D}] \exp\left(-\frac{\beta}{2} \sum_{links} \frac{D_l^2}{\epsilon_l} \right) \delta(\phi_N) \times \prod_{nodes}^{N} \exp(-i\phi \nabla \cdot \mathbf{D}). \tag{4}$$

The scalar field ϕ is conjugate to $\nabla \cdot \mathbf{D}$ and is associated with the nodes. We integrate over the field $\mathbf{D}$ in Eq. (4) and find an expression in terms of the field ϕ. From here on we assume $\beta = 1$, or equivalently we absorb the temperature in the units of energy.

$$\mathcal{Z} = \left(\prod_{links} \epsilon_l^{1/2} \right) \int \mathcal{D}(\phi) \delta(\phi_N) \exp\left(-\frac{1}{2} \sum_{links} \epsilon_l (\nabla \phi)^2 \right). \tag{5}$$

Equation (5) reduces the problem to that of calculating the partition function of a single scalar field with ϵ-dependent gradient energy [8]. The only subtlety is the δ-function term in the measure. We will see below that its effect is to remove the integration over the constant mode and to contribute an extra overall volume factor.

Equation (5) leads to a free energy containing several kinds of contribution. We wish to understand the lattice dependence of the various terms and remove those that diverge as we go to the continuum limit and scale as (V/s^3), where V is the volume and s the lattice spacing. What remains after taking care of these divergences corresponds to surface interactions [8,10]. To separate these contributions we rescale ϕ to $\frac{\phi}{\sqrt{\chi}}$ with χ an arbitrary positive function that is associated with nodes. Then, from Eq. (5),

$$\mathcal{Z} = \prod_{links} \epsilon_l^{1/2} \prod_{nodes} \frac{1}{\chi^{1/2}} \int \left(\prod_{nodes} d\phi \right) \delta\left(\frac{\phi_N}{\sqrt{\chi_N}} \right) \times \exp\left[-\frac{1}{2} \sum_{links} \epsilon_l \left(\nabla \frac{\phi}{\sqrt{\chi}} \right)^2 \right]. \tag{6}$$

We now focus our attention on the integral and on the remaining δ function. The first step is to recover simple Gaussian integrals by an orthogonal change of variable that makes the exponent diagonal. We write $\phi_n = \Sigma \alpha_{ni} a_i$, with n running over nodes, $i = 0 \ldots N-1$, and α_{ni} are expansion coefficients. Then, the integral in Eq. (6) becomes

$$I = \int \left(\prod_{i=0}^{N-1} da_i \right) \exp\left(-\sum_i \lambda_i \frac{a_i^2}{2} \right) \delta\left(\frac{1}{\sqrt{\chi_N}} \sum_i a_i \alpha_{iN} \right), \quad (7)$$

where the λ_i are the eigenvalues of the operator $\left(-\frac{1}{\sqrt{\chi}} \nabla \epsilon \nabla \frac{1}{\sqrt{\chi}}\right)$ and a_i are normalized eigenvectors. The lowest eigenvalue, $\lambda_0 = 0$, corresponds to the field configuration $\phi = N\sqrt{\chi}$, since for this configuration the gradient in the exponent acts on the constant vector. The normalized eigenvector is $\mathbf{V_0} = \frac{(\sqrt{\chi_1}, \sqrt{\chi_2}, \ldots, \sqrt{\chi_N})}{(\Sigma_i \chi_i)^{1/2}}$. Thus, the λ_0 expansion coefficient of ϕ_N is $\alpha_{0N} = \sqrt{\chi_N} / (\Sigma_i \chi_i)^{1/2}$.

We now integrate over a_0

$$I = \left(\sum_{nodes} \chi \right)^{1/2} \int \left(\prod_{i \neq 0} da_i \right) \exp(-\lambda_i a_i^2)$$

$$= \left(\sum_{nodes} \chi \right)^{1/2} \det{}^* \left(-\frac{1}{\sqrt{\chi}} \nabla \cdot \epsilon \nabla \frac{1}{\sqrt{\chi}} \right)^{-1/2}, \quad (8)$$

where the $\det^*$ indicates the product over nonzero eigenvalues. Thus

$$\mathcal{Z} = \left(\prod_{links} \epsilon_l^{1/2} \right) \left(\prod_{nodes} \frac{1}{\chi^{1/2}} \right) \left(\sum_{nodes} \chi \right)^{1/2} \times \det{}^* \left(-\frac{1}{\sqrt{\chi}} \nabla \cdot \epsilon \nabla \frac{1}{\sqrt{\chi}} \right)^{-1/2}. \quad (9)$$

We will now choose χ to factorize the partition function into extensive terms and nonextensive terms, separating the terms that diverge in the continuum limit from those that remain finite.

We specialize to the case of interfaces between uniform dielectric materials. We discretize as follows. When a vertex belongs to a slab of material, all three links departing in the positive direction from that vertex belong to the same slab. Thus, for a plane geometry, a slab of thickness $a=1$ contains one plane of L^2 vertices and $3L^2$ links. This definition is not left-to-right symmetric, but it is convenient for periodic boundary conditions, as a slab of thickness a of ϵ_1 on a background of ϵ_0 is the same as a slab of thickness $a' = L - a$ of ϵ_0 on a background of ϵ_1. We now chose χ as $\chi_n = \frac{1}{3}(\epsilon_{nx} + \epsilon_{ny} + \epsilon_{nz})$. For a system where ϵ is piecewise constant this implies choosing $\chi = \epsilon$.

From Eq. (9) we find the free energy, $\mathcal{F} = -\ln \mathcal{Z}$,

$$\mathcal{F} = -\frac{1}{2} \sum_{links} \ln \epsilon_l + \frac{1}{2} \sum_{nodes} \ln \epsilon_n - \frac{1}{2} \ln \left(\sum_{nodes} \epsilon_n \right) + \frac{1}{2} \ln \det{}^* \left(-\frac{1}{\sqrt{\epsilon}} \nabla \cdot \epsilon \nabla \frac{1}{\sqrt{\epsilon}} \right). \quad (10)$$

The choice $\chi = \epsilon$ leads to the last term in Eq. (10) which is homogeneous of degree zero in ϵ. Thus scaling all values of the dielectric constant by a factor leaves this contribution invariant. The other contributions contain ϵ dependent terms which scale as N, or $\ln N$, giving divergences as V or $\ln V$ in the infinite-volume limit. If we take the continuum limit keeping the volume finite, but sending the lattice spacing s to zero, these terms diverge as $1/s^3$ or $\ln s$. The determinant also has short-distance divergence in V, but this is independent of ϵ and it is the same for all systems. It arises from the short-distance behavior of the operator $-\epsilon^{-1/2} \nabla \cdot \epsilon \nabla \epsilon^{-1/2}$, which in all regions where ϵ is a smooth function of $\mathbf{r}$ is the same as the short-distance behavior of the operator $-\nabla^2$. This contribution is the free energy of the vacuum. It can be subtracted defining $\mathcal{F}_{reg} = \mathcal{F} - \frac{1}{2} \ln \det^*(-\nabla^2)$. In this paper we will be working with constant total volume, so this term can be ignored. We discuss these issues in detail in Sec. IV. The surface free energy is the last term in Eq. (10); it only contributes when ϵ varies at an interface. We therefore define

$$\mathcal{F}_{Surf} \equiv \frac{1}{2} \ln \left[\det{}^* \left(-\frac{1}{\sqrt{\epsilon}} \nabla \cdot \epsilon \nabla \frac{1}{\sqrt{\epsilon}} \right) \Big/ \det{}^* (-\nabla^2) \right]. \quad (11)$$

This interaction depends *only on the ratio* between the different dielectric constants of the uniform components of the physical system. For the water/lipid systems we wish to study this ratio is $\sim 1.7/80 \sim 50$, we can then equivalently choose in our numerical codes $\epsilon_1 = 50$ and $\epsilon_0 = 1$. Expression (11) is free of short-distance divergences in any region where $\epsilon(\mathbf{r})$ is smooth, since in those regions the short-distance behavior of the numerator and denominator of Eq. (11) are the same. However, if ϵ undergoes a sharp transition at a surface, there is an additional divergent contribution which can be ascribed to the self-energy of the interface between the two regions; a sharp interface affects modes of arbitrarily short wavelengths, therefore the large eigenvalue asymptotics of the numerator and denominator of Eq. (11) do not cancel. This divergence is qualitatively different from the volume divergences discussed earlier in this section. While the latter are the same in any continuum field theory and are usually dealt with using renormalization theory, the surface self-energy divergence is related to having defined the field theory on a *singular background* in which $\epsilon(r)$ is discontinuous [19,20]. In real physical systems treating the dielectric constant as discontinuous is an oversimplification; any transition between two materials occurs over a small, but finite, distance. On the lattice, the lattice spacing gives a natural cutoff and the contributions coming from the surface self-energy scale as $1/s^2$. In this work we focus on the interaction energy between *separate* surfaces, so we will subtract the surface self-energy by taking free energy differences between systems where the surfaces are rigidly translated but do not change shape.

Equation (10) is the fundamental equation we will use when extracting the surface interaction from the numerical results. We first determine the full partition function directly, either by matrix diagonalization, or by Monte Carlo simulation. Using Eq. (10) we extract the pure surface interaction, Eq. (11), by subtracting the extra terms in Eq. (10), which depend on the volume of the system and/or on the lattice. Explicitly,

$$\mathcal{F}_{Surf} = \mathcal{F} + \frac{1}{2} \sum_{links} \ln(\epsilon) - \frac{1}{2} \sum_{nodes} \ln(\epsilon) + \frac{1}{2} \ln \left(\sum_{nodes} \epsilon \right), \quad (12)$$

where for simplicity we do not include the vacuum contribution from $-\nabla^2$.

III. NUMERICAL EVALUATION OF FREE ENERGIES

We now compare two methods of evaluating the free energy, Eq. (10), of the discretized system. The first method is a direct evaluation of the determinant $\det^*\left(-\frac{1}{\sqrt{\chi}}\boldsymbol{\nabla}\cdot\boldsymbol{\epsilon}\boldsymbol{\nabla}\frac{1}{\sqrt{\chi}}\right)^{-1/2}$. The second is an implementation of the Monte Carlo algorithm, introduced in [21]. We consider a cubic box of side L, with periodic boundary conditions, with a cubic lattice of spacing $s=1$.

For small systems we evaluate the determinant $\det^*\left(-\frac{1}{\sqrt{\chi}}\boldsymbol{\nabla}\cdot\boldsymbol{\epsilon}\boldsymbol{\nabla}\frac{1}{\sqrt{\chi}}\right)^{-1/2}$ with standard matrix methods. If we set $\chi=1$, the partition function (9) then takes the form

$$\mathcal{Z}=\left(\prod_{links}\epsilon^{1/2}\right)L^{3/2}\det^*(-\boldsymbol{\nabla}\cdot\boldsymbol{\epsilon}\boldsymbol{\nabla})^{-1/2}. \tag{13}$$

We write the exponent in Eq. (5) as a symmetric matrix acting on the field ϕ, $\Sigma_{nodes}\phi_i M_{ij}\phi_j$, where the nonzero elements of M are given by

$$M_{i,i}=\sum_{nn=1}^{6}\epsilon_{i,nn},$$

$$M_{i,nn}=-\epsilon_{i,nn}, \tag{14}$$

where $\epsilon_{i,nn}$ indicates the value of the permittivity on the link connecting site i with the nearest neighbor in consideration. M is a symmetric matrix of dimension $L^3\times L^3$.

The determinant is calculated as the product of the eigenvalues of M, Λ_i. The free energy coming from $\det^*(-\boldsymbol{\nabla}\cdot\boldsymbol{\epsilon}\boldsymbol{\nabla})$ is

$$\mathcal{F}_{det}=+\frac{1}{2}\sum_{i=1}^{L^3-1}\ln\Lambda_i, \tag{15}$$

where now the sum extends only from $i=1$ to exclude the eigenvalue $\Lambda_0=0$. The free energy, from Eq. (13), is then

$$\mathcal{F}=\mathcal{F}_{det}-\frac{1}{2}\left(\sum_{links}\ln\epsilon-\ln(L^3)\right). \tag{16}$$

Comparing Eqs. (16) and (12), we see that the surface free energy is

$$\mathcal{F}_{surf}=\mathcal{F}_{det}-\frac{1}{2}\sum_{nodes}\ln\epsilon+\frac{1}{2}\ln\left(\sum_{nodes}\epsilon\right)-\frac{1}{2}\ln(L^3). \tag{17}$$

The last thing we need to take care is the constant, ϵ independent contribution $\ln\det^*(-\nabla^2)$, which was discussed in Sec. II, that represents the vacuum contribution (see also the Appendix for details). We can subtract this term by hand by computing it explicitly, or equivalently always consider free energy differences. We adopt the second strategy, so that the constant factor $\ln L^3$ entering in the last term of Eq. (17) can also be ignored.

As an alternative procedure, we have used the method of [21] to measure the free energy using thermodynamic integration and Monte Carlo simulation. We sample the partition function (2) using a collective worm algorithm [22] to update the field **D**. We obtain free energy differences between two systems: the one under study, and a reference system. In order to avoid surface divergences, the reference system has to be chosen as a rigid translation of the original system. In the example of parallel planar slabs, that we are going to analyze in detail, we take as "reference" the system where the surfaces are at maximum distance (i.e., $L/2$, in periodic boundary conditions).

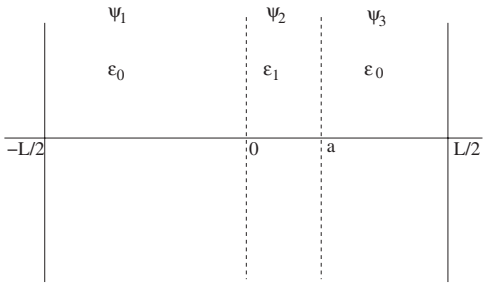

FIG. 1. One slab geometry.

The free energy obtained by the simulation, $\mathcal{F}_{sim}$, gives directly an evaluation of the left-hand side of Eq. (10). Using Eq. (12), we conclude that the surface contribution is

$$\Delta\mathcal{F}_{surf}=\Delta\mathcal{F}_{Sim}-\Delta\left[-\frac{1}{2}\sum_{links}\ln(\epsilon)+\frac{1}{2}\sum_{nodes}\ln(\epsilon)-\frac{1}{2}\ln\left(\sum_{nodes}\epsilon\right)\right]. \tag{18}$$

IV. ANALYTIC RESULTS

The above discretization methods can be applied in arbitrary geometry. To calibrate them we will apply them to a flat slab, and compare the results with an analytic expression for the surface free energy, Eq. (11), in the continuum limit. We consider a single-slab piecewise uniform system, periodic along the direction perpendicular to the slab, and infinite in the two transverse directions. Its geometry is shown in Fig. 1. Analytical results are well known for the similar system which is infinite in all three directions [8–10], but, to our knowledge, the result we derive here for the periodic system is new.

Starting from the constrained partition function on the continuum, Eq. (1), we derive the free energy of the periodic system following a procedure similar to [9,10]. However, our derivation does not extract the classical result as a limit of a quantum system; it considers the classical system from the start. We believe that in such treatment the physics is more transparent and we are able to better control issues such as subtraction of divergences which, as we have seen, are important for the comparison of the analytical results with numerical data. In particular, since the final expression we derive is free of divergences, but the starting point, Eq. (1), is not, we have to make sure that the finite quantities we calculate are consistent with the corresponding finite quantities defined on the lattice and computed through the numerical methods. We will show that expression (11) is essentially finite (i.e., up to the—unphysical—divergent surface self-

energy that appears in singular backgrounds, that will be discussed separately), so it is meaningful to compare it with numerical results.

We will compute the free energy per unit transverse area. This quantity stays finite in the limit of infinite transverse size, and is defined, following Eq. (11),

$$\mathcal{F}_{Surf} = \frac{1}{2L_t^2} \ln \frac{\det^*(-\epsilon^{-1/2} \nabla \epsilon \nabla \epsilon^{-1/2})}{\det^*(-\nabla^2)} \tag{19}$$

$$= \frac{1}{2L_t^2} [\mathrm{Tr}^* \ln(-\epsilon^{-1/2} \nabla \epsilon \nabla \epsilon^{-1/2}) - \mathrm{Tr}^* \ln(-\nabla^2)], \tag{20}$$

$$\equiv \tilde{\mathcal{F}} - \mathcal{F}_0, \tag{21}$$

where L_t is the linear dimension of the system along the uniform directions, and the limit $L_t \to \infty$ is understood.

Determinants are cyclic invariant so that $\det(-\epsilon^{-1} \nabla \epsilon \nabla)$ is equivalent to $\det(-\epsilon^{-1/2} \nabla \epsilon \nabla \epsilon^{-1/2})$. In our test case, we find it more convenient to evaluate

$$\tilde{\mathcal{F}} = \frac{1}{2L_t^2} \mathrm{Tr}^* \ln(-\epsilon^{-1} \nabla \epsilon \nabla). \tag{22}$$

Let us consider the geometry in Fig. 1, with $\epsilon(\mathbf{r})$ piecewise constant. We take our system to be periodic on $(-\frac{L}{2}, \frac{L}{2})$. The surface of the slabs are perpendicular to the z axes. We separate the eigenvalue equation writing $\psi(x,y,z) = e^{i\rho_x x + i\rho_y y} \psi_z(z)$, with

$$\epsilon^{-1}(\epsilon\rho^2 - \partial_z \epsilon \partial_z)\psi_z = \Lambda \psi_z \tag{23}$$

and $\rho^2 = \rho_x^2 + \rho_y^2$.

The eigenfunction along z is taken separately in the three regions,

$$\psi_\alpha(z) = A_\alpha e^{ipz} + B_\alpha e^{-ipz}, \tag{24}$$

with $\alpha = 1,2,3$. Integrating the eigenvalue equation over a small interval we find that ψ satisfies the same boundary conditions as the scalar electrostatic potential ϕ:

$$\psi_-(z) = \psi_+(z), \tag{25}$$

$$\epsilon_- \partial \psi_-(z) = \epsilon_+ \partial \psi_+(z), \tag{26}$$

which are derived by integrating Eq. (23) across the boundaries. Here, + and − refer to the left- and right-hand side of the interface.

Equation (23) gives $\rho^2 + p^2 = \Lambda$ and $\rho^2 + q^2 = \Lambda$, from which we immediately deduce $p = q$. Moreover, we notice that Λ has to be real and positive. Indeed, consider an $\epsilon(\mathbf{r})$ everywhere positive, with the eigenvalues equation $-(\nabla \epsilon \nabla)\psi = \epsilon \Lambda \psi$. Then, $0 \leq \int \epsilon |\nabla \psi|^2 = -\int \psi^* (\nabla \epsilon \nabla)\psi - \int \nabla [\psi^* (\epsilon \nabla \psi)]$. The last integral is zero because of the matching condition (26), leaving us with $0 \leq -\int \psi^* (\nabla \epsilon \nabla)\psi = \Lambda \int \epsilon |\psi|^2$. As a consequence q has to be either real or purely imaginary, and in the latter case $|q| \leq \rho$.

Inserting the functions (24) in the eigenvalue equation (23) and using the boundary conditions, we find

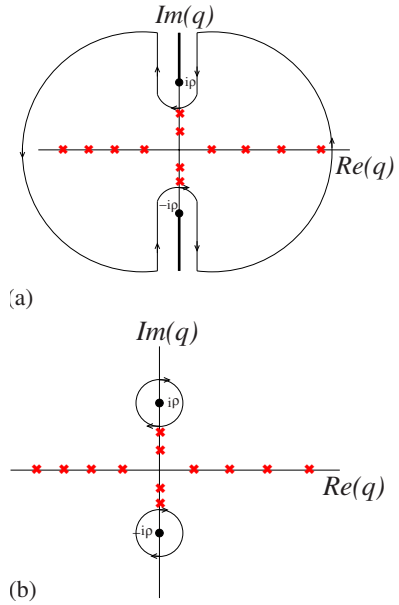

FIG. 2. (Color online) (a) Contour of integration. The zeros of $Q(q)$ are the big X's. (b) Contour after integration by parts.

$$\left(\frac{\epsilon_1 - \epsilon_0}{\epsilon_1 + \epsilon_0}\right)^2 \frac{1 - \cos[q(L-2a)]}{1 - \cos(qL)} = 1. \tag{27}$$

This equation determines the eigenvalues q_n of the effective one-dimensional eigenvalue problem, Eq. (23). The surface contribution to the free energy per unit area from Eq. (22) is [27]

$$\tilde{\mathcal{F}} = \frac{1}{2L_t^2} \mathrm{Tr} \ln[-\epsilon^{-1}(\epsilon \nabla_t^2 + \partial_z \epsilon \partial_z)] = \frac{1}{8\pi^2} \int_0^\infty d^2\rho \frac{1}{2} \sum_n \ln(\rho^2 + q_n^2), \tag{28}$$

where q_n's are the solutions of Eq. (27). The extra factor 2 in the integrand of the last expression comes from the consideration that the transformation $q \to -q$ leaves both Eq. (27), and the wave function (24), invariant up to a renaming of the coefficients. Summing over all solutions of Eq. (27) requires dividing by 2 to avoid double counting. An equation similar to Eq. (28) holds for $\mathcal{F}_0$ that we need to subtract, with the q_n's replaced by the appropriate eigenvalues for the uniform system.

In the Appendix we show that the free energy, Eq. (20), can be written in terms of a "spectral function" on the complex q-plane, $Q(q)$

$$\mathcal{F}_{surf} = \tilde{\mathcal{F}} - \mathcal{F}_0 = \frac{1}{16\pi^2} \int_0^\infty d^2\rho \oint_\gamma \frac{dk}{2\pi i} \ln(\rho^2 + k^2) \frac{Q'(k)}{Q(k)}, \tag{29}$$

where the integration contour γ encloses all the complex solutions of the eigenvalue equation (27), for example the path shown in Fig. 2(a), chosen in such a way that it avoids the branch cuts $(-i\infty, -i\rho)$ and $(i\rho, +i\infty)$ from the logarithm. For the single-slab configuration, the appropriate function is

$$Q(q) = 1 - \left(\frac{\epsilon_1 - \epsilon_0}{\epsilon_1 + \epsilon_0}\right)^2 \frac{1 - \cos[q(L-2a)]}{1 - \cos(qL)}. \quad (30)$$

As shown in the Appendix, this choice corresponds to subtracting the energy of uniform empty space, the second term in Eq. (20).

To arrive at an explicit expression for Eq. (29), we first rewrite the argument of the ρ integral,

$$f(\rho) = \oint_\gamma \frac{dk}{2\pi i} \ln(\rho^2 + k^2) \frac{Q'(k)}{Q(k)}. \quad (31)$$

Rather than evaluating directly $f(\rho)$, let us calculate its derivative,

$$\frac{d}{d\rho} f(\rho) = \oint_\gamma \frac{dk}{2\pi i} \frac{2\rho}{\rho^2 + k^2} \frac{Q'(k)}{Q(k)} = \oint_\gamma \frac{dk}{2\pi i} \frac{2\rho}{\rho^2 + k^2} \frac{d}{dk} \ln Q(k). \quad (32)$$

The integral along the large circle at infinity vanishes, and the only nonzero contribution comes from the paths along the imaginary axis. We deform the contour to two circles enclosing the two poles in $\pm i\rho$, as shown in Fig. 2(b).

Equation (32) is evaluated using the residue theorem

$$\frac{df}{d\rho} = \frac{d}{d\rho} \ln Q(i\rho) + \frac{d}{d\rho} \ln Q(-i\rho), \quad (33)$$

whence

$$f(\rho) = 2 \ln Q(i\rho) + 2\bar{f}, \quad (34)$$

where $\bar{f}$ is an integration constant, and we have used $Q(q) = Q(-q)$. Inserting Eq. (34) in Eq. (20), we obtain

$$\mathcal{F}_{Surf} = \frac{1}{4\pi} \int_0^\infty \rho \ln Q(i\rho) d\rho + \frac{\bar{f}}{4\pi} \int_0^\infty \rho d\rho. \quad (35)$$

The last term is still quadratically divergent. If we introduce a cutoff ω in momentum space, the last integral is $O(\bar{f}\omega^2)$, the same scaling as a short-distance surface divergence. This is the explicit manifestation of the divergent surface self-energy described in Sec. III, and it is caused by the singular background, characterized by a sharp transition in the dielectric profile. This divergence can be subtracted by setting the integration constant $\bar{f}=0$, as it does not depend on the dielectric constants. Notice however that the divergence will depend, in general, on the shape of the surfaces considered, so if we want to compare the free energies of systems whose interfaces have different geometries, we must treat this divergence more carefully. The self-energy can be interpreted as the *finite tension* of the surface interface, and one has to take it into account if one wishes to treat the surfaces *dynamically*.

Setting the last term in Eq. (35) to zero we find

$$\mathcal{F}_{Surf} = \frac{1}{4\pi} \int_0^\infty \rho \ln Q(i\rho) d\rho. \quad (36)$$

Equation (36) is gives us the free energy once we know the eigenvalue equation. In the Appendix we show how the choices we made uniquely determine the function $Q(q)$ as its zeros correspond to the solutions of the eigenvalue equation, and its poles correspond to the eigenvalues of the uniform system. These two requirements are equivalent to asking that the subtraction we performed to arrive at Eq. (36) is exactly the second term in Eq. (20).

Using Eq. (30), the surface free energy becomes

$$\mathcal{F}_{Surf} = \frac{1}{4\pi} \int_0^\infty \rho \ln \left[1 - \left(\frac{\epsilon_1 - \epsilon_0}{\epsilon_1 + \epsilon_0}\right)^2 \frac{1 - \cosh[\rho(2a-L)]}{1 - \cosh(\rho L)} \right] d\rho. \quad (37)$$

The integral over ρ is finite for separations $a>0$; the integrand varies as $\rho e^{-2a\rho}$ for large ρ. Thus the surface free energy, Eq. (11), is free of short-distance divergences and can be used in numerical computations.

In the limit $L \to \infty$, Eq. (37) reduces to [8,23] $\mathcal{F}_{Surf} = \frac{1}{4\pi} \int_0^\infty \rho \ln\left[1 - \left(\frac{\epsilon_1 - \epsilon_0}{\epsilon_1 + \epsilon_0}\right)^2 e^{-2\rho a}\right] d\rho$. The method of this section and the Appendix can be extended to systems composed of an arbitrary number of slabs through the use of transfer matrices [23].

V. NUMERICAL RESULTS

We used both matrix diagonalization and Monte Carlo simulation to study the slab geometry of Sec. IV in order to calibrate the numerical methods and evaluate discretization errors. We first consider a volume $V=12^3$ with lattice spacing $s=1$. The dielectric constant of the slab is $\epsilon_1=2$ with background dielectric constant $\epsilon_0=1$. These values of ϵ *do not correspond to any interesting physical system*, and are far from the 1:50 ratio we seek when studying water/lipid systems. However one of the methods with which we wish to compare (Monte Carlo simulation) becomes inefficient for large dielectric contrasts. It is thus more convenient to work with reduced contrast in order to compare results.

The matrix diagonalization is performed using the built in methods of MATLAB. It requires about one minute on a 2 GHz workstation to calculate the free energy as a function of the gap G, with $G=1,\ldots,11$. The Monte Carlo simulation was run with 40 points for the thermodynamic integration. For each gap measuring the free energy requires about one hour of simulation. Figure 3 shows that the agreement between the two methods is within error bars.

The difference in computer resources needed in these two calculations of the free energy shows that Monte Carlo is not the best method for studying the large distance tails of the interaction between dielectric media. The surface interactions we want to measure are three to four orders of magnitude smaller than the self-energy; their extraction requires extremely precise measures which are hard to achieve with statistical evaluations. We can estimate the scaling of the

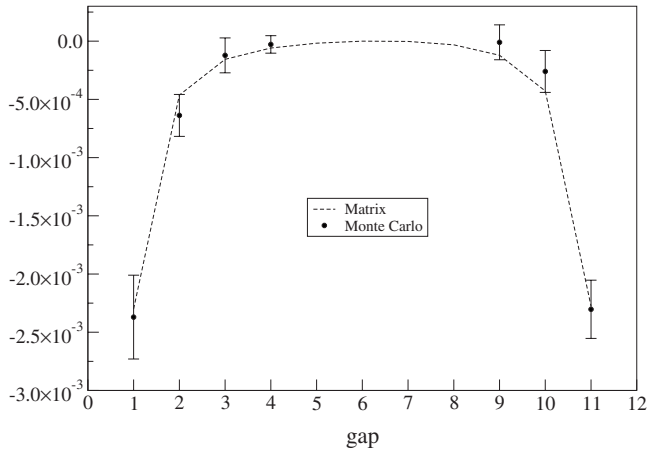

FIG. 3. $\Delta\mathcal{F}_{Surf}$ as a function of surface separation from matrix diagonalization (solid) and Monte Carlo (points). The free energy is measured in arbitrary units where the lattice spacing is taken to be 1. The system size $L=12$, ratio between the dielectric constants is $\epsilon_0:\epsilon_1=1:2$. The reference system is taken to be a system with maximal slab thickness, i.e., $a'=L/2$.

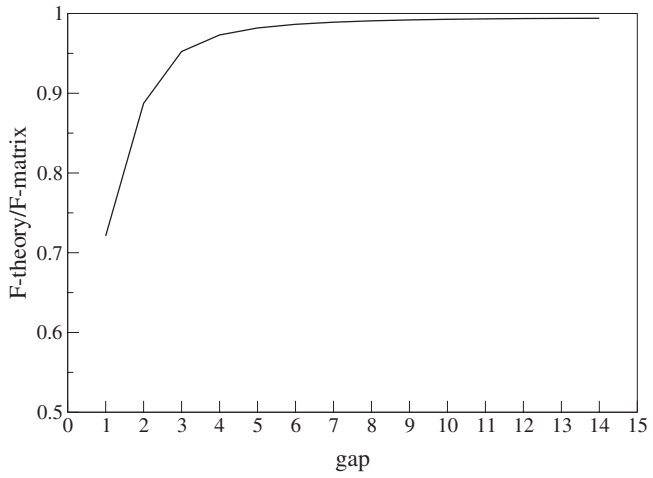

FIG. 4. Ratio of $\mathcal{F}_{th}$ computed from the analytic formula, Eq. (37), and $\mathcal{F}_m$ calculated from the matrix. The transverse dimensions are $L_x=L_y=60$, while the longitudinal direction is $L_z=30$. For this system $\epsilon_0:\epsilon_1=1:50$.

resources needed in Monte Carlo as follows: The interaction between two interfaces scales as $L^2/G^2=O(1)$, which is to be compared to the volume free energy which scales as $O(V)$. Thus we require $O(V^2)$ Monte Carlo sweeps of cost $O(V)$ to generate statistically useful results for a single integration point. In addition, as the system size grows, more simulations points are needed for the thermodynamic integration. Considering all these factors, we see that the Monte Carlo method requires an effort that scales worse than L^9.

Matrix diagonalization is not affected by statistical noise. The complexity is dominated by the evaluation of the determinant: $O(V^3)=O(L^9)$ with dense matrix routines. The real constraint for matrix diagonalization turns out to be the memory required for holding dense matrices. With 1 GB memory available for computation, using standard routines, the largest system size we can consider is $L_{max}\sim 25$; memory usage scales as $O(V^2)=O(L^6)$. In order to study larger, more interesting systems we now specialize to objects which are translationally invariant in one direction. Because of the symmetry one can then use Fourier analysis to simplify the numerical problem. When we do this we find that we need only find the eigenvalues of a matrix of dimensions $L^2\times L^2$ instead of $L^3\times L^3$.

We write $\phi=\Sigma_{q_z}\phi_z^{(q_z)}\phi_{xy}^{(q_z)}$, where $\phi_z^{(q_z)}$ are plane waves with $q_z=2\pi n/L$ and $n=0,1,\ldots,L$, corresponding to the eigenvalue $2[1-\cos(q_z)]$ on a periodic lattice. Using this form for the eigenfunctions we find

$$\phi M\phi=\sum_{q_z}\phi_{xy}^{(q_z)}\tilde{M}(q_z)\phi_{xy}^{(q_z)} \tag{38}$$

where the nonzero elements of the reduced matrix $\tilde{M}(q_z)$ take the form

$$\tilde{M}_{i,i}(q_z)=\sum_{nn=1}^{4}\epsilon_{i,nn}+2\epsilon_z[1-\cos(q_z)],$$

$$\tilde{M}_{i,nn}(q_z)=-\epsilon_{i,nn}, \tag{39}$$

and $\ln\det^* M=\Sigma_{q_z}\ln\det^*\tilde{M}(q_z)$. The sum over nearest neighbors runs only along the x and y axes, ϵ_z indicates the value of ϵ along the uniform direction z. Using this approach, the new limit in size due to memory constraints becomes $\tilde{L}_{max}=L_{max}^{3/2}\sim 125$. However, in this case, computing time becomes the ultimate limiting factor because the determinant evaluation has to be performed L times, once for each q_z, requiring an effort $O(L^7)$. A system size of about $L=50$ is the largest system we can consider on our same 2 GHz processor, which leads to evaluating the determinant in about one hour.

We used this technique to compare the result obtained with matrix methods to our analytical calculations. Our analytic result, Eq. (37), is valid in the limit that the transverse directions of the system are large compared to the longitudinal direction. We thus study a system of dimensions $60\times 60\times 30$, where the smaller number refers to the longitudinal direction, and compare it to Eq. (37) for $\epsilon_1=50$ and $\epsilon_0=1$. Results are shown in Fig. 4 where we have plotted the ratio of the analytical result over numerical result as a function of surface separation. We see that the agreement is rather poor for the smallest separations, as might be expected in a discretized system. For larger gaps the agreement significantly improves.

We now use the Fourier-matrix method to study the interaction between parallel grooves in dielectric surfaces. Using microfabrication techniques such grooves are easy to manufacture; recent theoretical studies have investigated the effects of corrugations on quantum Casimir free energies [11,24]. We also note that one can study the Casimir energy as a function of lateral phase shift between the groove corrugations. Experimental evidence for lateral force was presented in [25].

For sinusoidal grooves analytic results were found using a second-order perturbation in the amplitude parameter, while

for rectangular grooves an exact numerical solution was found. The effect of corrugation wavelength and amplitude in relation to surface separation was investigated and it was found that for corrugation lengths much bigger than gap G, proximity force approximation (PFA) works well while in the limit of corrugation lengths much smaller than the amplitude, a small distance regime is reached [26]. The first correction term to the parallel plate free energy, $\delta=\mathcal{F}/\mathcal{F}_{flat}-1$, was determined. It was found that in the limit of the corrugation length $\lambda \gg G$ the correction δ to the Casimir energy depends only on the corrugation amplitude, and it is proportional to G^{-1}. In the opposite situation of $\lambda \ll G$ the correction to the energy depends on both wavelength and amplitude and $\delta \sim G^{-2}$.

Our numerical approach is valid for any groove profile, or indeed with any $2+1$ dimensional interfacial profile, and for all separation regimes. We first consider the interaction of rectangular groove and a planar interface. We analyzed the dependence of the free energy on the corrugation wavelength λ and on the surface separation G. In accordance to the analytical results for quantum Casimir, in the limit $\lambda \gg G$ we find the proximity force approximation gives results in agreement with our numerical results. According to this widely used approximation, one considers the interaction of a small portion of the surface with a corresponding portion on the other surface which sits vertically above, assuming the surface is locally flat. The interaction between the two "plaquettes" is taken as the interaction of two parallel surfaces at the same vertical distance, and the contribution from all plaquettes is then added to obtain the total interaction. In a system of $V=40^3$, for the particular case of groove depth $H=4$, and gap $G=6$, at maximal wavelength $\lambda=20$ the agreement between the PFA prediction and the direct numerical result is around 90%. As λ becomes smaller and comparable to the gap, the agreement drops to less than 20%. We have also investigated the free energy behavior in the limit $\lambda \ll G$. We have indications that, as in the quantum system, the correction term δ goes as $1/G$, but in order to be more certain one would need to study a larger system where ratios $G/\lambda \sim 10^2$ can be reached.

We now consider a sinusoidal groove, Fig. 5, with system size $L=46$, amplitude of oscillation $a=6$, wavelength L. The minimal distance G_{min} between the grooves is reached when their relative phase is π, and is equal to 1. In this configuration the vertical distance between the surfaces varies from $G_{min}=1$ to $G_{max}=25$. The shift S is measured in units of the lattice spacing as the displacement from the position where the grooves are perfectly aligned. Letting the top groove shift laterally over the bottom groove from the $S=L/2$ configuration (shown in Fig. 5) we measure the free energy as a function of the shift, $\mathcal{F}(S)$. $\mathcal{F}(S)$ gives information about lateral Casimir forces. When looking at the effect of the shift one expects the free energy to vary because the distribution of vertical distances changes as one groove is laterally displaced. Indeed when the shift is zero all the points of the opposing grooves have the same distance $2a+G_{min}$, while for $S=L/2$, the distance between any two vertically aligned points varies from G_{min} to $G_{max}=G_{min}+4a$. But beside this projection of the vertical Casimir interaction along the direction of the displacement, one expects to also detect lateral

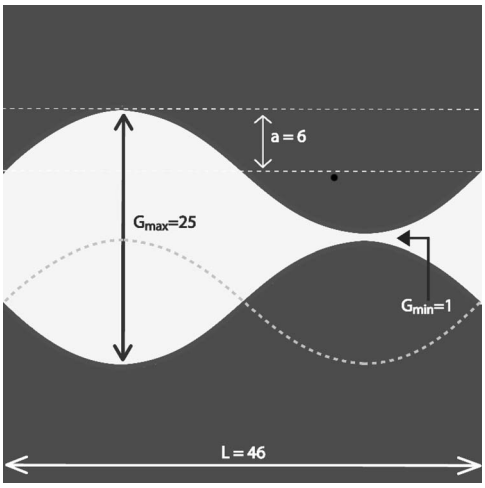

FIG. 5. Large sinusoidal grooves at $S=L/2$. The dashed profile indicates the position of the lower surface in the configuration $S=0$.

interactions between curved surfaces. Due to the nonadditivity of Casimir forces, and because of the large deformation of the groove with respect to the flat geometry, these two contributions cannot be disentangled. In Fig. 6 we present the results obtained with the reduced matrix diagonalization method, that gives the global interaction, and compare it to PFA, that only considers the effect of the *local* vertical displacement. PFA underestimates the free energy by factors that vary from around 10% when the grooves are mirroring (phase shift π), up to 40% for phase shifts close to zero. This is what one would expect since PFA fails to consider collective effects, which are more important when larger positions of the surfaces are close. These violations of the proximity force approximation are not peculiar to the classical regime and similar effects are also found for the quantum system for significantly nonflat geometries [11,12].

VI. CONCLUSIONS

We have presented a formulation of fluctuation induced interactions between dielectrics discretized to a lattice. We analyzed how the contributions to the on-lattice partition function depend on the discretization and on the volume, and we have derived an appropriate definition for the surface interaction, which stays finite in the continuum limit. We compared two numerical methods to compute the free energy of surface interactions. The first is a direct evaluation of the matrix determinant. The second is a Monte Carlo simulation together with thermodynamic integration.

While the constrained partition function allows the simulation of systems including full long-ranged Casimir interaction it turns out to be a rather inefficient method for extracting the asymptotic interactions between bodies. The nonextensive surface interactions are rather easily lost in statistical noise. We consider that the use of matrix methods has considerable promise. Already interesting problems can be studied in the $2+1$ dimensional translationally invariant systems, such as grooves, or blades. We note that we have only

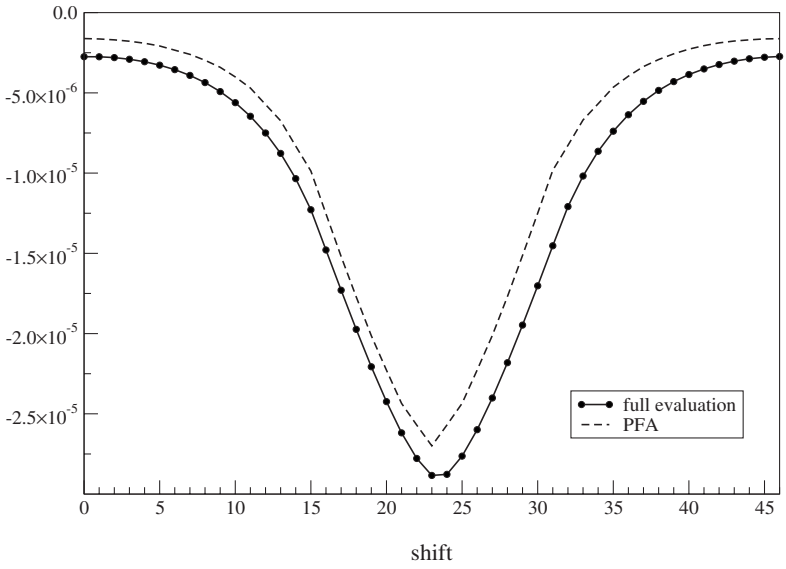

FIG. 6. Free energy as a function of phase shift measured in arbitrary units where the lattice spacing is equal to 1. For this system the ratio between the dielectric constants is 1:50.

used the simplest dense matrix methods. We anticipate that the use of more specialized sparse matrix solvers should allow the study of larger physical systems, without the requirement of translation invariance in one dimension.

Generalizations including the study of more elaborate dielectric functions that include scale dependent dielectric response [17] as well as quantum effects will be presented in future papers.

ACKNOWLEDGMENTS

We would like to thank R. L. Jaffe and R. Golestanian for comments and discussion. This work was partially supported by Volkswagenstiftung, by ANR Grant No. NT05-1-41861, INTAS Grant No. 03-51-6346, RTN Contract Nos. MRTN-CT-2004-005104 and MRTN-CT-2004-503369, CNRS PICS Grant Nos. 2530 and 3059, and by an European Excellence Grant No. MEXT-CT-2003-509661. F.N. acknowledges support of the European Commission Marie Curie Actions Contract No. MEIF-CT-2006-039369.

APPENDIX: REGULARIZATION OF ULTRAVIOLET DIVERGENCES

In this appendix we analyze the short-distance divergences in the parallel plate geometry discussed in Sec. IV. We address the subtraction of divergent vacuum energy and the divergent surface self-energy, showing that the latter arises from the singular nature of the background.

In the continuum limit, there is always an ϵ-independent divergent contribution in the free energy which arises from the existence of modes of ϕ with arbitrarily large momentum. To see this, consider a system where ϵ is everywhere uniform. The free energy corresponding to $\det^*(-\nabla^2)$ diverges as

$$\mathcal{F} \sim \frac{1}{2}\sum_n \ln \lambda_n, \quad \lambda_n \sim n^2. \tag{A1}$$

This divergence corresponds to large-momentum modes; it is present in the single-slab system analyzed in Sec. IV, as the eigenvalues in Eq. (27) also grow indefinitely.

Consider now the free energy before the subtraction, Eq. (28),

$$\tilde{\mathcal{F}} = \frac{1}{2L_t^2}\mathrm{Tr}^* \ln(-\epsilon^{-1}\nabla\,\epsilon\,\nabla) \tag{A2}$$

$$= \frac{1}{8\pi^2}\int_0^\infty d^2\rho \frac{1}{2}\sum_n \ln(\rho^2 + q_n^2). \tag{A3}$$

We now write the summation as a contour integral in the complex plane using Cauchy's theorem,

$$\sum_n \ln(\rho^2 + q_n^2) = \oint_\gamma \frac{dk}{2\pi i} \ln(\rho^2 + k^2)\frac{\tilde{Q}'(k)}{\tilde{Q}(k)}, \tag{A4}$$

where the spectral function $\tilde{Q}(q)$ has simple zeros [28] for $q=q_n$, and the integral is over an appropriate contour γ that encloses all zeros of $\tilde{Q}(q)$. We have used the fact that whenever $\tilde{Q}(q)$ has a simple zero, $\tilde{Q}'/\tilde{Q}$ has a simple pole with unit residue. Equation (A4) is clearly ill defined, since the argument of the summation becomes arbitrarily large.

Notice that, if $\tilde{Q}(q)$ has a pole of order p at $q=\bar{q}$, Eq. (A4) is invalid, since close to $\bar{q}$ we have

$$\frac{\tilde{Q}'(q)}{\tilde{Q}(q)} \sim -\frac{p}{(q-\bar{q})} \tag{A5}$$

and we obtain an extra contribution to the right-hand side. So, even formally, expression (A4) holds only if the spectral function has zeros corresponding to the eigenvalues of the problem at hand, and no other zeros *nor poles*. However we can see from Eq. (A5) that introducing simple poles $\bar{q}_n$ in the spectral function is equivalent to *subtracting* the free energy $\bar{\mathcal{F}}$ of a system that has eigenvalues $\bar{q}_n$. In this case therefore we formally have

$$\sum_n \ln(\rho^2+q_n^2)-\sum_m \ln(\rho^2+\bar{q}_m^2)=\oint_\gamma \frac{dk}{2\pi i}\ln(\rho^2+k^2)\frac{Q'(k)}{Q(k)}, \tag{A6}$$

where now $Q(q)$ has q_n as zeros and $\bar{q}_m$ as poles. Depending on the properties of the spectral function, it can happen that the two terms on the left-hand side are infinite, but the integral on the right-hand side is finite, so that the expression (A6), corresponding to the difference in free energies, is meaningful.

Thus, the free energy difference between a given system and the vacuum can be written using Eq. (A6), in which

$$Q(q)=\frac{\tilde{Q}(q)}{Q_0(q)}, \tag{A7}$$

where the zeros of $\tilde{Q}(q)$ and of $Q_0(q)$ are the solutions of the eigenvalue equations of the system under consideration and of the vacuum, respectively, and neither function has other zeros or poles. Using Eqs. (A3) and (A6) we arrive at

$$\tilde{\mathcal{F}}-\mathcal{F}_0=\frac{1}{16\pi^2}\int_0^\infty d^2\rho\oint_\gamma \frac{dk}{2\pi i}\ln(\rho^2+k^2)\frac{Q'(k)}{Q(k)}, \tag{A8}$$

i.e., Eq. (29) in Sec. IV.

For a uniform system in a periodic box of size L the eigenvalues are $q_n=\frac{2n\pi}{L}$, so we can choose, for example [29],

$$Q_0(q)=\cos(qL)-1. \tag{A9}$$

For the single-slab system considered in Sec. IV, the eigenvalue equation (27) fixes $\tilde{Q}(q)$ up to an overall constant, which can be in turn set by the requirement that $\tilde{Q}(q)$ reduces to $Q_0(q)$ when $\epsilon_1=\epsilon_0$,

$$\tilde{Q}(q)=\left(\frac{\epsilon_1-\epsilon_0}{\epsilon_1+\epsilon_0}\right)^2\{1-\cos[q(2a-L)]\}-[1-\cos(qL)]. \tag{A10}$$

The resulting spectral function,

$$Q(q)=\tilde{Q}(q)/Q_0(q)=1-\left(\frac{\epsilon_1-\epsilon_0}{\epsilon_1+\epsilon_0}\right)^2\frac{1-\cos[q(L-2a)]}{1-\cos(qL)}, \tag{A11}$$

coincides with the one given in Eq. (30), which as shown in Sec. IV, when used in Eq. (A8) gives a finite result for the surface free energy, up to a (subleading) divergence in the surface tension which will be discussed below.

In Sec. IV we found that we had to subtract an additional divergence that can be traced to the integration constant introduced in Eq. (33). This originates from Eq. (A8) being still ill defined; only its derivative with respect to ρ is finite. In general however, there are situations when one can evaluate Eq. (A8) directly and obtain a finite result. This is the case when $Q'(k)/Q(k)$ vanishes sufficiently fast for large $|k|$. Under this assumption, let us go back to the contour integration along the path shown in Fig. 3(a); we can neglect the integration over the large circle already at the level of Eq. (A8), and integrate by parts in the remaining contribution along the cuts

$$f(\rho)=\oint_{cut}\frac{dk}{2\pi i}\ln[(\rho^2+k^2)]\frac{Q'(k)}{Q(k)}$$
$$=-\oint_{cut}\frac{dk}{2\pi i}\ln Q(k)\frac{2k}{\rho^2+k^2}, \tag{A12}$$

At this point, the branch cuts $(-i\infty,-i\rho)$ and $(i\rho,-i\infty)$ have disappeared, and we can again deform the contour to the two circles enclosing the two poles in $\pm i\rho$, as shown in Fig. 2(b). Then the residue theorem gives

$$f(\rho)=2\ln Q(i\rho), \tag{A13}$$

which leads to the finite result, Eq. (36). Notice that this procedure fails in the example of Sec. IV, since $Q(k)$ defined in Eq. (30) does not have the required property for large $|k|$.

The key observation is that, as we showed earlier in this appendix, $Q(k)$ must be defined in such a way as to subtract the leading vacuum energy divergence, so that

$$Q(k)=\frac{\tilde{Q}(k)}{Q_0(k)}, \tag{A14}$$

where $Q_0(k)$ is a function giving the vacuum eigenvalue distribution, and $\tilde{Q}(k)$ is such that first it gives the eigenvalue distribution of the system under consideration and second it reduces to $Q_0(k)$ for a uniform system. In all physical situations, *the large momentum modes should always behave the same as in the vacuum beyond a certain threshold*, determined by the properties of the material under investigation. Therefore it is natural to assume that in all physical systems, $Q(k)\to 1$ as $|k|\to\infty$, which automatically guarantees that $Q'(k)/Q(k)\to 0$ for large $|k|$. In the case of a single plane slab, it is unphysical to assume that the dielectric constant changes discontinuously, because that would imply that *all modes*, with arbitrary short wavelength, are affected by the presence of the interface, as one can see from the matching conditions (26). It is more reasonable to assume that modes with wavelengths shorter than a certain cutoff δ (the molecular or atomic scale of the dielectric) will not be sensitive to the difference between the dielectric and the vacuum, therefore $Q(k)\sim 1$ for modes with $|k|>1/\delta$. Following these considerations it is clear that the divergence in the surface self-energy in Sec. IV is exclusively related to the singular nature of the background under consideration, and that in a physical system with a smooth dielectric function $\boldsymbol{\epsilon}(\mathbf{r})$ the free energy in Eq. (11) is finite.

[1] H. B. K. Casimir, Proc. K. Ned. Akad. Wet. **51**, 793 (1948).
[2] I. E. Dzyaloshinskii, E. M. Lifshitz, and L. P. Pitaevskii, Adv. Phys. **10**, 165 (1961).
[3] J. N. Israelashvili and D. Tabor, Prog. Surf. Membr. Sci. **7**, 1 (1973).
[4] K. A. Milton, J. Phys. A **37**, R209 (2004).
[5] B. Ninham and V. Parsegian, Biophys. J. **10**, 646 (1970).
[6] V. Parsegian and B. Ninham, Biophys. J. **10**, 664 (1970).
[7] R. Netz, Eur. Phys. J. E **5**, 189 (2001).
[8] D. S. Dean and R. R. Horgan, Phys. Rev. E **71**, 041907 (2005).
[9] N. G. V. Kampen, B. R. Nijboer, and K. Schram, Phys. Lett. **26A**, 307 (1968).
[10] B. W. Ninham and V. A. Parsegian, J. Chem. Phys. **52**, 4578 (1970).
[11] R. Buscher and T. Emig, Phys. Rev. A **69**, 062101 (2004).
[12] H. Gies and K. Klingmüller, Phys. Rev. Lett. **96**, 220401 (2006).
[13] J. Feinberg, A. Mann, and M. Revzen, Ann. Phys. **288**, 103 (2001).
[14] S. Pasquali and A. C. Maggs, e-print arXiv:0704.2171.
[15] A. Rodriguez, M. Ibanescu, D. Iannuzzi, J. D. Joannopoulos, and S. G. Johnson, Phys. Rev. A **76**, 032106 (2007).
[16] B. W. Ninham and J. Daicic, Phys. Rev. A **57**, 1870 (1998).
[17] A. C. Maggs and R. Everaers, Phys. Rev. Lett. **96**, 230603 (2006).
[18] A. C. Maggs and V. Rossetto, Phys. Rev. Lett. **88**, 196402 (2002).
[19] M. P. Hertzberg, R. L. Jaffe, M. Kardar, and A. Scardicchio, Phys. Rev. Lett. **95**, 250402 (2005).
[20] R. L. Jaffe, e-print arXiv:hep-th/0307014.
[21] I. Pasichnyk, R. Everaers, and A. Maggs, URL http://www.pct.espci.fr/~tony/lifshitz/igor.pdf
[22] L. Levrel and A. C. Maggs, Phys. Rev. E **72**, 016715 (2005).
[23] B. W. Ninham and V. A. Parsegian, J. Chem. Phys. **53**, 3398 (1970).
[24] T. Emig, A. Hanke, R. Golestanian, and M. Kardar, Phys. Rev. A **67**, 022114 (2003).
[25] F. Chen, U. Mohideen, G. L. Klimchitskaya, and V. M. Mostepanenko, Phys. Rev. Lett. **88**, 101801 (2002).
[26] T. Emig, Europhys. Lett. **62**, 466 (2003).
[27] The replacement $L_t^2 \to (2\pi)^{-2}$ is understood by writing down the trace as a sum of diagonal terms on the eigenfunction $\psi_{q,p}$ with the operators depending on the two transverse momenta ρ and ρ', and integrating over ρ'. We find an infrared divergence of the form $\delta^2(0)$ which can be regularized introducing a cutoff in the positions. This gives a multiplicative factor $(L_t/2\pi)2$.
[28] In case of zeros of order p, the the right-hand side must be multiplied by $1/p$.
[29] Notice that this function has zeros of order $p=2$. This introduces the same extra factor $1/2$ as in Eq. (A3).